Influence of Sm_2O_3 microalloying and Yb contamination on Y211 particles coarsening and superconducting properties of IG YBCO bulk superconductors

L Vojtkova[1] ⓘ**, P Diko**[1]**, J Kovac**[1] **and M Vojtko**[2]

[1] Institute of Experimental Physics, Slovak Academy of Sciences, Watsonova 47, 040 01 Košice, Slovakia
[2] Institute of Materials Research, Slovak Academy of Sciences, Watsonova 47, 040 01 Košice, Slovakia

E-mail: vojtkova@saske.sk

Abstract

Single grain $YBa_2Cu_3O_{7-x}$ (YBCO or Y123) bulk superconductors were produced by an infiltration growth process. The solid phase precursor was prepared by solid state synthesis from $Y_2O_3 + BaCuO_2$ powders. The influence of the addition of Sm_2O_3 and YB contamination from the substrate on the microstructure and superconducting properties was analyzed. The dependences of Yb concentration on the distance from the bottom of the samples measured by energy dispersive spectroscopy microanalysis used in conjunction with scanning electron microscopy confirmed the contamination of the samples during the melting stage of the sample preparation. It is shown that the addition of Sm in low concentration and its combination with Yb from the substrate modify the coarsening of the Y211 particles as well as lead to the appearance of a secondary peak effect in the field dependences of the critical current density.

Keywords: YBCO superconductors, chemical pinning, ytterbium contamination, samarium addition, infiltration growth, *in situ* synthesized solid phase, superconductors properties

(Some figures may appear in colour only in the online journal)

1. Introduction

REBCO (where RE—rare earth element) bulk single-grain superconductors prepared using an infiltration growth (IG) method have almost the same dimensions of the resultant sample as the starting precursors. This property is very important in the preparation of the samples for real applications. The study of these materials is focused on improving the superconducting properties and understanding the mechanisms of the formation of their microstructure [1–8].

The latest results show that samples prepared by the synthesis of Y211 (Y_2BaCuO_5) solid phase by reaction (1):

$$Y_2O_3 + BaCuO_2 \rightarrow Y_2BaCuO_5 \qquad (1)$$

exhibit small Y211 particles in Y123 matrix even without the addition of CeO_2 or Pt [1, 3]. Besides, they have sufficient porosity [9] and are suitable for the standard oxygenation

process. Small Y211 particles in Y123 matrix have a positive influence on the critical current density in a zero magnetic field [10–13]. It has already been shown that the size of Y211 particles can also be influenced by microalloying with RE elements (doping) in concentrations below 1 wt.%. Doping with RE elements may lead to substitutions into the Y123 crystal lattice that induce the so-called chemical pinning associated with the appearance of a secondary peak at higher fields with the dependence of the critical current density, J_c, on the applied magnetic field, B [14–18]. The Yb_2O_3 substrate which is used to retard grain nucleation at the bottom of the sample can also be the source of chemical pinning by the pollution of the sample by Yb [19].

In our previous work [20] we showed that RE doping into YBCO single grain bulks can influence both coarsening of Y211 particles and chemical pinning. In this work, the microstructure, contamination from the substrate, and
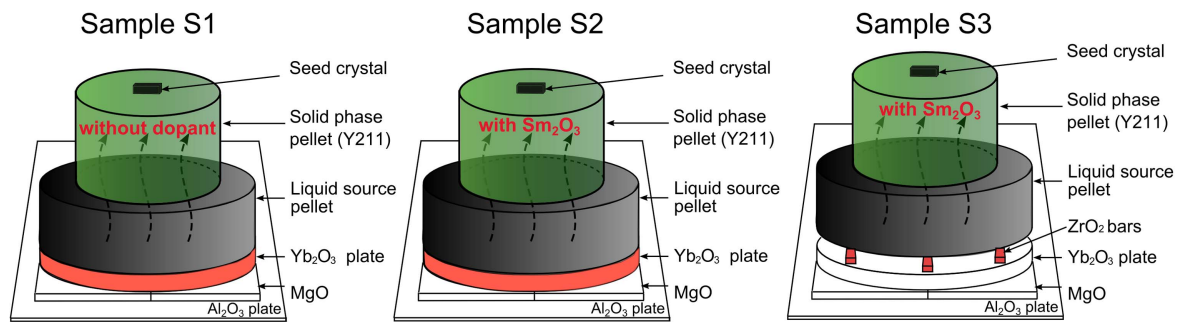
Figure 1. Schematic arrangements of YBCO bulk superconductors produced by an IG method without/with the addition of Sm_2O_3 (S1/S2, S3, respectively) and with a Yb_2O_3 substrate plate for samples S1, S2, and ZrO_2 bars for sample S3.
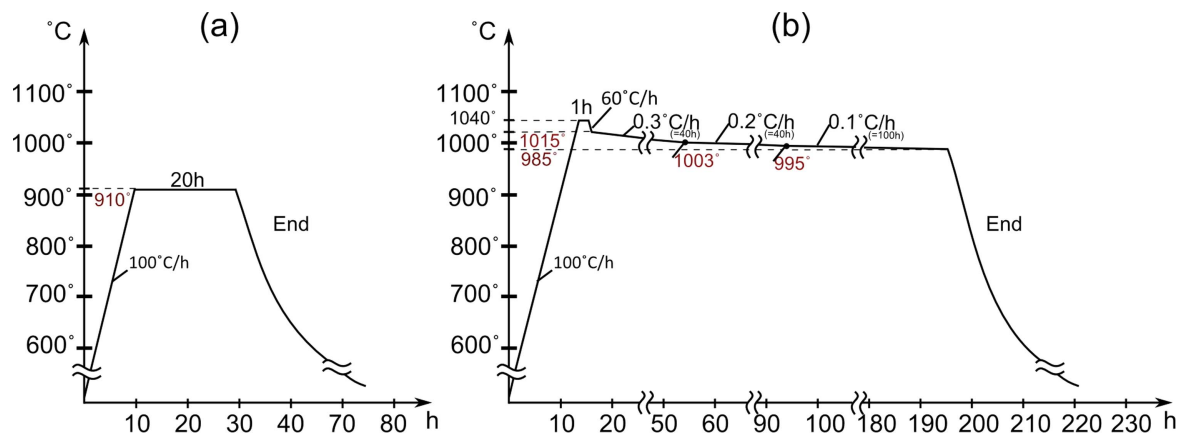

Figure 2. Time–temperature schedule of single crystal preparation using an IG method: (a) for synthesizing the Y211 solid phase pellet; (b) for the crystal growth process from the seeds.

superconducting properties of single grain YBCO bulk superconductors prepared by an IG process were analyzed. The influence of Sm microalloying and the composition of the layers in the crystal growth experiments on Yb contamination, coarsening of Y211 particles, transition temperature, and field dependence of critical current density at 77 K were studied.

2. Experimental materials and methods

2.1. Preparation of sample layers

The samples were produced using an IG method. The solid phase pellet (Y211 pellet) was synthesized from the mixture of $Y_2O_3 + 1.2 \cdot BaCuO_2$ powders. This ratio was chosen according to the work in [9]. Sm dopant in the form of Sm_2O_3 powder in the quantity 0.21 wt.% was added into the precursor of the solid phase before synthesis [17]. The powders were mixed for 20 min and then uniaxially pressed under pressure of 6 MPa into a cylindrical form with a 20 mm diameter and a weight of 12 g.

The precursor of the liquid phase pellet consisted of the mixture of powders in the ratio of $Y_1Ba_2Cu_3O_{7-x}$: $3 \cdot BaCuO_2$: $2 \cdot CuO$. The powders were mixed for the same amount of time as the solid phase precursor. Mixed powders in the amount of 16.5 g were pressed into a cylindrical form

with a 32 mm diameter, under the same conditions as in the previous case.

The thinner solid phase pellet precursor was put onto the thicker liquid phase pellet. Precursor pellets of sample S1 without dopant and sample S2 with the addition of Sm_2O_3 were placed on the Yb_2O_3 substrate plates. In the case of sample S3, ZrO_2 bars were inserted between the liquid source pellet and Yb_2O_3 layer. The solid and liquid phase pellets with the Yb_2O_3 substrate plate were put on single-crystalline MgO laying on an Al_2O_3 plate. In order to ensure epitaxial growth of the crystals, Sm123 single crystal seeds were placed in the center on the top of the whole assembly. Schematics of the arrangements of the layers used to produce the YBCO bulk superconductors are shown in figure 1.

2.2. Heat treatment

The precursors of the Y211 solid phase pellet were sintered for 20 h at 910 °C according to equation (1). A time–temperature diagram of the heat treatment of the solid phase pellet is shown in figure 2(a).

The growth of single crystals was realized in accordance with time–temperature schedule presented in figure 2(b). The process started with heating the samples to the maximum temperature $T_m = 1040\,°C$, at a heating rate of 100 °C/h, at which point the liquid phase was formed and infiltrated into the solid phase pellet during 1 h. Then, the system was cooled to near peritectic temperature 1015 °C at a rate of 60 °C/h,
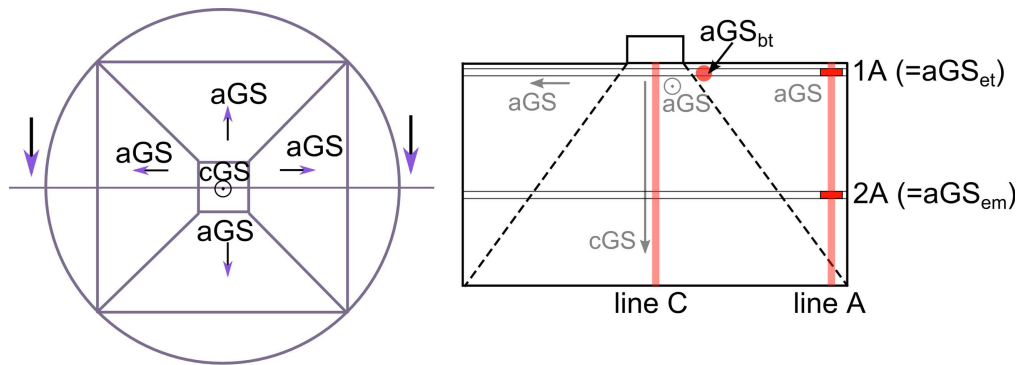
2

Figure 3. Schematic of crystal growth directions and sectors (left) and cutting out of the samples (right) for the measurements of the superconducting properties (1A, 2A). Line A and C represent the measurement of Yb concentration in the sample. Microstructure photos were made at the positions indicated by red marks in the aGS: aGS_{bt}—at the beginning of the aGS near the seed; aGS_{et}—at the end top in the area 1A; aGS_{em}—at the end of a = GS and in the middle of the sample rim (area 2A).
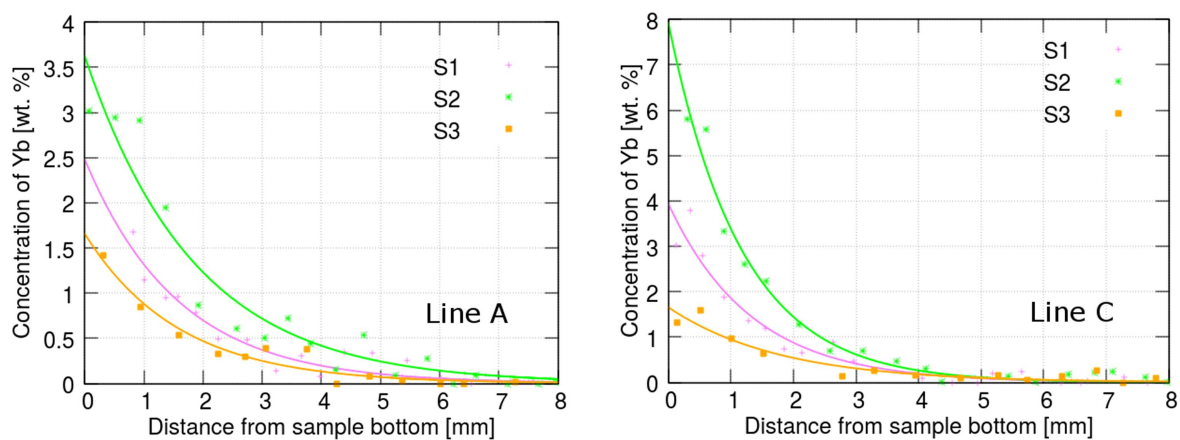

Figure 4. Dependence of Yb concentration in the Y123 + Y211 mixture on the distance from the sample bottom.

and the samples were slowly cooled through the peritectic temperature over 180 h. The cooling rate was decreased in three steps (0.3 °C/h; 0.2 °C/h; 0.1 °C/h) and subsequently the samples were cooled in a furnace to room temperature (figure 2(b)).

2.3. Preparation of the samples for the measurement of the superconductor properties

To measure the superconductive properties of the samples with and without the addition of Sm_2O_3 and to investigate the effect of the Yb_2O_3 substrate on the system, the samples were cut out in two places: first 1A—at the end of the a-growth sector (aGS) near the top surface (figure 3 (1A-position)); second 2A—at the end of the aGS but at its middle (figure 3 (2A-position)). The samples were cut out with dimensions of approximately 1.5 × 1.5 × 0.5 mm (a × a × c directions, respectively). Subsequently a small specimen was oxygenated in flowing oxygen at 410 °C for 200 h.

The measurements of the transition temperature T_c and critical current density J_c were performed using a vibrating sample magnetometer (VSM) magnetometer at liquid nitrogen temperature. The critical transition temperature to the superconducting state was estimated from the curves of the magnetic transition (1 mT). The critical current density values

were calculated from the measurements of the magnetic loop by means of an extended Bean mode [21].

The composition of the samples and quantitative analysis of ytterbium penetration from the substrate into the crystal at line A and C from bottom to top (figure 3) was analyzed by energy dispersive spectroscopy (EDS) used in conjunction with scanning electron microscopy (SEM).

The microstructure of the samples was observed with an optical microscope in polarized light. The size distribution of the Y211 particles was evaluated from the obtained images using image analysis software.

3. Results and discussion

3.1. Microstructure

As the studied samples were grown on the Yb_2O_3 substrate, we checked the ytterbium contamination of the samples. Quantitative analysis of ytterbium penetration from the substrate into crystal was performed along line A and C (figure 3), and the dependences of Yb concentration as a function of the distance from the bottom of the grown YBCO single-grain sample are presented in figure 4. All three dependences have a typical diffusion profile and prove that
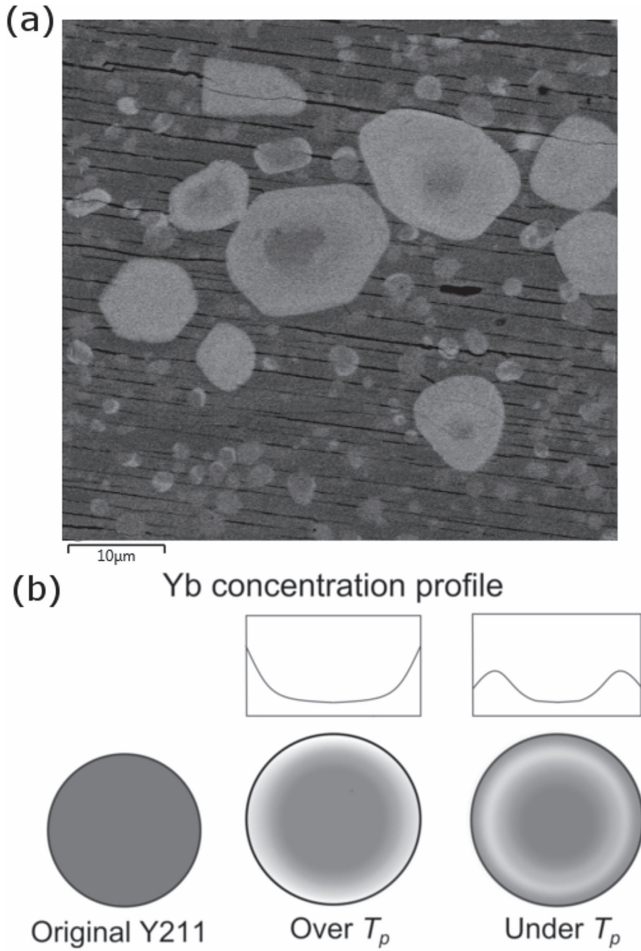
(a)

(b) Yb concentration profile

Original Y211   Over T_p Under T_p

Figure 5. Local EDS analysis of sample S1 at the sample bottom (a) and schematic representation of enrichment processes of Y211 particle with ytterbium from the Yb_2O_3 substrate which take place above peritectic temperature, T_p, and depletion of the 211 particle surface at the crystal growth below peritectic temperature (b).

Yb diffused through the melt in the melting stage to the sample. The concentration of Yb is below the resolution limit of EDS (0.1 wt.%) at the distance of about 6 mm from the seed for the measurement along the C line and about 7 mm for measurement along the A line; this is apparently caused by the fact that the parts at the rim of the sample were in the melted state for a longer time. We suppose that corresponding but low concentration of Yb will be present also at the top surface of the samples. The maximum measured Yb concentration is obviously at the sample bottom surface. The lowest Yb concentration at the bottom surface was measured in sample S3 with ZrO_2 bars placed between the liquid source pellet and Yb_2O_3 layer (figure 1). For samples S1 and S2 this value is higher.

Our measured Yb concentrations are the sum of Yb content in the Y123 phase and Yb content in the Y211 phase. Therefore we measured Yb concentration in the Y211 and Y123 phases close to the sample bottom. The microstructure of sample S1 close to the bottom surface is presented in figure 5. In a back scattered electron mode of the SEM image, a higher concentration of Yb is reflected by higher brightness

because the atomic mass of Yb is higher than that of Y (atomic mass: Y = 88.91 amu, Yb = 173.0 amu). One can see that more Yb is present in the 211 particles than in the 123 phase. In both phases, Yb substitutes for Y in the crystal lattice. Apparently, Yb diffused through the melt to the Y211 particles, and the surface parts of Y211 particles were converted into a $(Y,Yb)_2BaCuO_5$ solid solution. The microstructure in figure 5 shows that larger 211 particles contain more Yb than smaller ones. The middle parts of the 211 particles are dark, and EDS analysis of a large 211 particle confirmed that its central part does not contain Yb at all. The highest Yb concentration was measured in the bright part of a large 211 particle at 1.8 wt.%. The measured concentration of Yb in the 123 phase was 0.8 wt.%.

During the formation of YBCO bulk crystal by the peritectic reaction:

$$((Y, Yb)_2BaCuO_5)_S + (3BaO \cdot 5CuO \cdot y((Y, Yb)O_{1.5}))_L$$
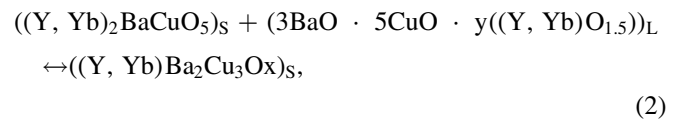
$$\leftrightarrow ((Y, Yb)Ba_2Cu_3Ox)_S, \tag{2}$$

where symbol S means solid and symbol L means liquid, Y and Yb from the (Y, Yb)211 particles are participating in the formation of the (Y, Yb)123 crystal.

Sm and Yb may influence the coarsening of the Y211 particles by the Ostwald ripening process and trapping/pushing of the 211 particles by the growing 123 crystal. Therefore we analyzed the microstructure of the samples in three different positions in the aGS (figure 6) with a supposed different concentration of Yb and constant concentration of Sm (samples S2 and S3). In all positions, some amount of largeY211 particles is present but the microstructure in those positions differs mainly in the size of smaller Y211 particles. The quantitative data of the Y211 particle size, d_{211}, and the 211 volume percentage, V_{211}, for all analyzed positions are presented in table 1. The dependence of the size of smaller Y211 particles on the position in the a-GS is shown in figure 7. It can be seen that the position in the sample has a significant influence on the size of small 211 particles mainly in the samples with the addition of Sm (S2 and S3). The observed size of the 211 particles can be related to competition of two processes. The first process is a growth of the 211 particles with the time in melted state by Ostwald ripening mechanism. The second process is a decrease of the critical 211 particle size for pushing with increasing undercooling, i.e. higher growth rate.

The inclusion trapping/pushing theory [22] proposes that when a sample solidifies at a certain growth rate, R_1, inactive inclusion particles smaller than a certain critical radius, r^* are not trapped in the solid but are instead excluded. At a higher growth rate, R_2, inclusion of particles with the radius of r^* are then trapped. The relation between the growth rate, R^*, and the critical radius, r^*, is predicted by

$$R^* = \Delta\sigma_0 / \eta r^{*n}, \tag{3}$$

where $\Delta\sigma_0 = \Delta\sigma_{sp} - \Delta\sigma_{sl} - \Delta\sigma_{pl}$. The interface energy between the solid phase and the inclusion particle is
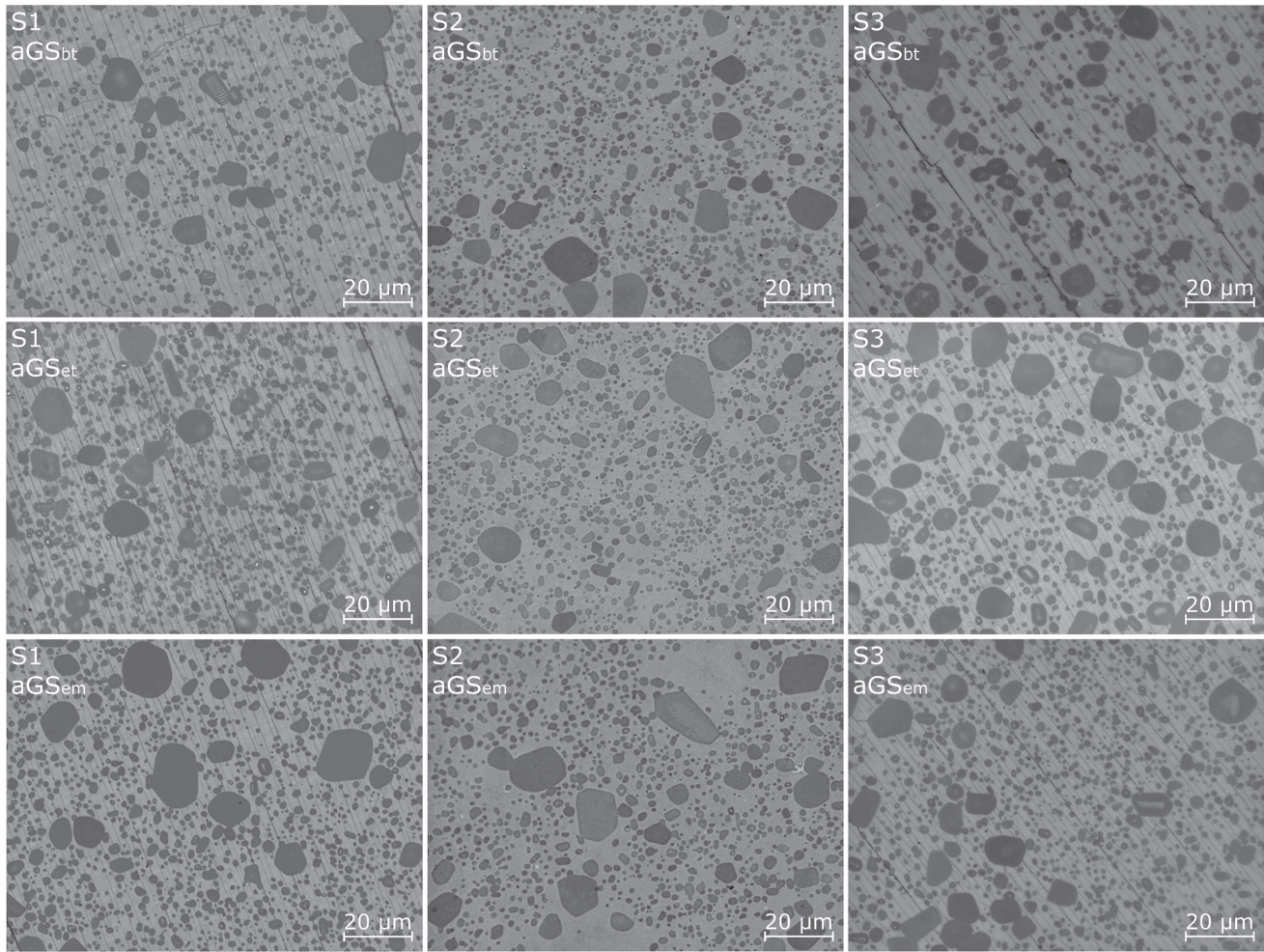
Figure 6. Polarized light optical micrographs from the polished halve sample section parallel to the a/c-plane. Positions on the section: aGS$_{bt}$—beginning of the aGS at the top sample surface, aGS$_{et}$—end of the aGS at the top sample surface (position 1A), aGS$_{em}$—end of the aGS in the middle of the sample rim (position 2A).

represented by $\Delta\sigma_{sp}$, $\Delta\sigma_{sl}$ represents the interface energy between the solid phase and the liquid phase, and $\Delta\sigma_{pl}$ represents the interface energy between the inclusion particle and the liquid phase; η is the viscosity coefficient of the liquid phase and n is a constant between 1 and 2. This theory has been successfully applied to the trapping/pushing phenomena in the solidification of the 123–211 system [23]. The growth rate R is proportional to the undercooling ΔT. The samples presented were grown at a slow cooling rate, and thus the undercooling and the growth rate increased with the distance from the seed. The result should be an increase of V211 with distance from the seed and a decrease of d_{211}.

The Ostwald ripening process also depends on the interface energy between a 211 particle and the peritectic melt, L_p, [24] by

$$d^3_t - d^3_0 \approx DC\sigma t, \qquad (4)$$

where d_t is the final and d_0 is the starting 211 particle size, D is the diffusion coefficient of Y in the peritectic melt L_p, C is the Y concentration in the melt, σ is the 211/L_p interface energy, t is the holding time.
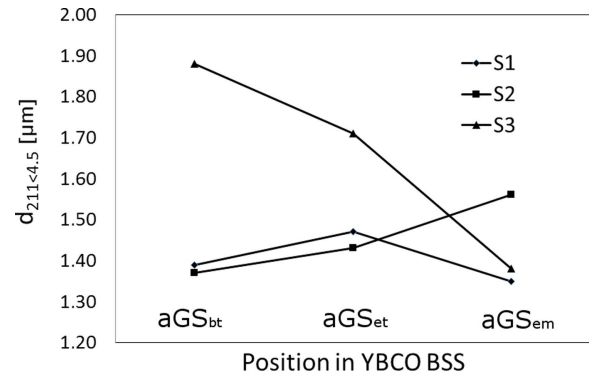

Figure 7. Dependence of the size of the 211 particles larger than 4.5 mm, $d_{211>4.5}$, on the position in the aGS. Positions: aGS$_{bt}$—beginning of the aGS at the top sample surface, aGS$_{et}$—end of the aGS at the top sample surface (position 1A), aGS$_{em}$—end of the aGS in the middle of the sample rim (position 2A).

The presence of Sm and Yb in the studied samples can influence 211/L_p interface energy as well as the viscosity of the peritectic melt. The measured size of the 211 particles, $d_{211>4.5}$, in different positions is then the result of Yb and Sm concentration at different positions of the growing 123

Table 1. Data of the measurement of mean size, d_{211}, and volume percentage, V_{211}, of the Y211 particles in the aGS. Positions in the sample: bt—beginning of the aGS at the top sample surface, et—end of the aGS at the top sample surface (position A1), em—end of the aGS in the middle of the sample rim (position A2).

| Sample	S1						S2						S3					
Measured value	d_{211} [μm]			V_{211} [%]			d_{211} [μm]			V_{211} [%]			d_{211} [μm]			V_{211} [%]		
Position in aGS	bt	et	em	bt	et	em	bt	et	em	bt	et	em	bt	et	em	bt	et	em
All Y211	1.54	1.63	1.48	26.55	32.24	35.65	1.46	1.54	1.70	35.15	36.24	35.97	2.17	2.17	1.55	32.43	43.16	32.54
Y211 < 4.5 μm	1.39	1.47	1.35	16.31	19.76	21.84	1.37	1.43	1.56	25.41	25.23	22.99	1.88	1.71	1.38	18.51	17.18	19.56
Y211 > 4.5 μm	7.22	7.39	7.92	10.24	12.48	13.80	8.35	7.77	8.37	9.74	11.02	12.98	6.7	8.16	7.43	13.92	25.98	12.99
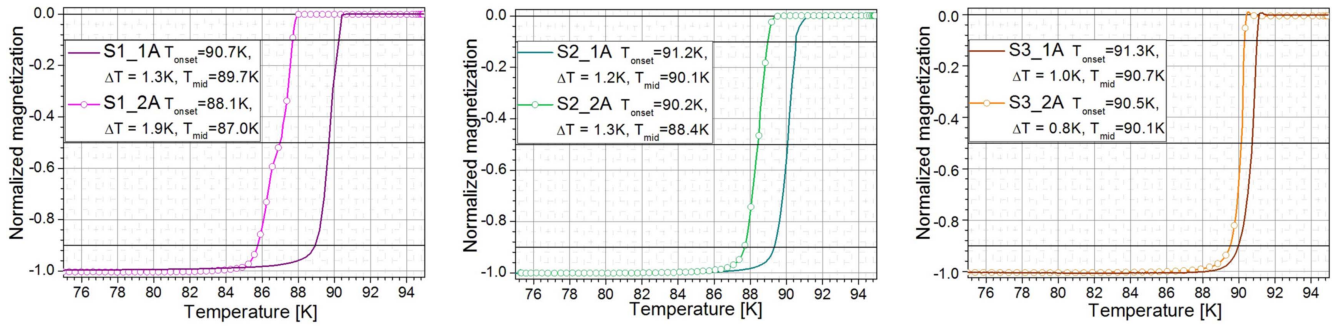
Figure 8. The temperature dependence of magnetization for samples S1 (without Sm doping), S2 (Sm doping), and S3 (Sm doping, ZrO_2 bars).
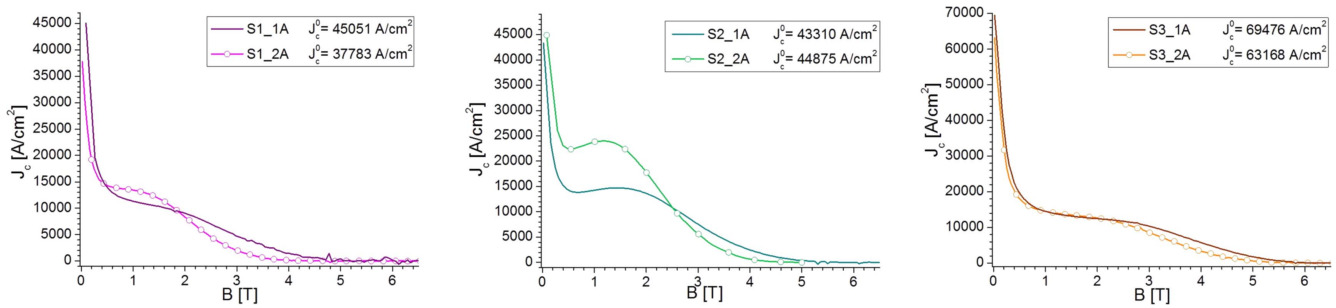

Figure 9. J_c-B dependences at 77 K for samples S1 (without Sm doping), S2 (Sm doping), and S3 (Sm doping, ZrO_2 bars).

crystal. In the sample without Sm doping (S1) and the highest Yb contamination the size of the 211 particles is influenced only by Yb from the substrate, and the observed dependence of the 211 size on the position in the sample suggests that the concentration of Yb is close to optimum. In the sample S3 with Sm doping, the contamination by Yb at the beginning of crystallization is too low (figure 4) and the 211 particles are larger (figure 7, position aGS$_{bt}$). Increasing contamination with longer time in the melted state (figure 7 position aGS$_{et}$) and the position closer to the Yb$_2$O$_3$ substrate (figure 7, position aGS$_{em}$) in this sample leads to the lower size of the 211 particles suggesting some optimum Sm + Yb concentration. In the sample S2 with higher Yb contamination (figure 4), the Sm + Yb concentration is apparently increasing above optimal, and that causes coarsening of the 211 particle.

3.2. Superconducting properties

The measured values of the critical current density J_c at 77 K and transition temperature T_c for the positions 1A (aGS$_{et}$) and 2A (aGS$_{em}$) are presented in figures 8 and 9, respectively. The values of the critical current density were evaluated from magnetic loop measurements by means of an extended Bean model.

The analyzed samples exhibit differences in the transition to superconducting state and in the field dependences of critical current density. The sample S1 without Sm doping has a higher T_c at the aGS$_{et}$ position ($T_c = 89.7$ K, $\Delta T_c = 1.3$ K)

where we may expect lower Yb contamination than at the aGS$_{em}$ position ($T_c = 87.0$ K, $\Delta T_c = 1.9$ K). Higher Yb contamination even leads to double T_c like behavior suggesting the presence of two 123 phases with different Yb concentration (figures 8, 2A).

Higher Yb contamination is also reflected in a more pronounced peak effect in the field dependence of the critical current density at 77 K and lower irreversibility field (figure 9, S1) for the aGS$_{em}$ position. The sample S2 with Sm doping and Yb contamination exhibits nicely pronounced secondary peak effects for both measured positions (figure 9). The highest J_c at 1.5 T reaching $2.5 \cdot 10^4$ A cm^{-2} was measured for the aGS$_{em}$ position in this sample. Similar to the sample S1, higher Yb contamination leads to a lower irreversibility field. It is interesting that the T_c values at the measured positions are higher in this sample than in sample S1; this may be caused by some interaction of Sm and Yb dopants. The sample S3 with Sm doping and lower Yb contamination has the highest values of T_c and the highest J_c values at zero field reaching $6.9 \cdot 10^4$ A cm^{-2} (figure 9). The T_c and irreversibility field values in this sample are the highest for the position with the supposed lowest Yb contamination, and both of them only slightly decrease with higher Yb contamination.

The observed behavior of the superconducting properties suggest that some optimum Sm and Yb concentration and Sm/Yb ratio may exist for obtaining required superconducting properties.

4. Conclusions

Quantitative characterization of the microstructure, Yb impurities, and superconducting properties of single grain YBCO bulk superconductors microalloyed with Sm prepared by an IG process were studied. It was shown that:

- The contamination of samples from the Yb_2O_3 substrate exhibits diffusion like dependence of Yb concentration on the distance from the sample bottom. The contamination is influenced by Sm doping and by the insertion of a ZrO_2 interlayer placed between the liquid source pellet and Yb_2O_3 substrate.
- At melting stage, Yb is concentrated in the 211 particles.
- The size of the 211 particles in the 123 bulk single crystal is influenced by both Sm dopant and Yb contamination, through the influence of trapping and growth of 211 particles.
- Optimum combination of added Sm and Yb contamination leads to the most pronounced secondary peak effect and to the highest critical current density in a higher magnetic field.
- Observed double T_c like behavior suggests inhomogeneity of Yb distribution in the 123 phase.

ORCID iDs

L Vojtkova ⦿ https://orcid.org/0000-0001-9026-8198

References

[1] Devendra Kumar N, Shi Y, Palmer K G, Dennis A R, Durrell J H and Cardwell D A 2016 A novel, two-step top seeded infiltration and growth process for the fabrication of single grain, bulk (RE)BCO superconductors *Supercond. Sci. Technol.* **29** 0950101–11

[2] Chen P-W, Chen I-G, Chen S-Y and Wu M-K 2011 The peak effect in bulk Y-Ba-Cu-O superconductors with CeO_2 doping by the infiltration growth method *Supercond. Sci. Technol.* **24** 0850211–8

[3] Liu Y, Pan B, Xiang H, Qian J, Du G, Huang S, Yao X, Izumi M and Wang Y 2017 $YBa_2Cu_3O_{7-\delta}$ superconductor bulks composited by Y_2BaCuO_5 nanoparticles derived from homogeneous nucleation catastrophe *J. Am. Ceram. Soc.* **100** 3858–64

[4] Iida K, Hari Babu N, Shi Y and Cardwell D A 2005 Seeded infiltration and growth of large, single domain Y–Ba–Cu–O bulk superconductors with very high critical current densities *Supercond. Sci. Technol.* **18** 1421–7

[5] Yang W M and Wang M 2013 New method for introducing nanometer flux pinning centers into single domain YBCO bulk superconductors *Phys. C: Supercond.* **493** 128–31

[6] Devendra Kumar N, Missak Swarup Raju P, Pavan Kumar Naik S, Rajasekharan T and Seshubai V 2014 Effect of Ag addition on the microstructures and superconducting properties of bulk YBCO fabricated by directionally solidified preform optimized infiltration growth process *Phys. C: Supercond. Appl.* **496** 18–22

[7] Muralidhar M, Ide N, Koblischka M R, Diko P, Inoue K and Murakami M 2016 Microstructure, critical current density and trapped field experiments in IG-processed Y-123 *Supercond. Sci. Technol.* **29** 054003 1–10

[8] Muralidhar M, Kenta N, Zeng X L, Koblischka M R, Diko P and Murakami M 2016 Record critical current densities in IG processed bulk $YBa_2Cu_3O_y$ fabricated using ball-milled $Y_2Ba_1Cu1O_5$ phase *Phys. Status Solidi* A **213** 443–9

[9] Vojtkova L and Diko P 2017 Microstructure YBCO bulk superconductors fabricated by infiltration growth process *Mater. Sci. Forum* **891** 489–93

[10] Fujimoto H, Murakami M, Nakamura N, Gotoh S, Kondoh A, Koshizuka N and Tanaka S 1991 Critical current properties of YBCO prepared by melt processes *Advances in Superconductivity IV Proc. 4th Int. Symp. on Superconductivity (ISS '91)* pp 339–42

[11] Mahmood A, Park S D, Jun B H, Youn J S, Han Y H, Sung T H and Kim C J 2009 Improvement of the superconducting properties of an infiltrated YBCO bulk superconductor by a $BaCeO_3$ addition *Phys. C: Supercond.* **469** 1165–8

[12] Diko P 2000 Growth-related microstructure of melt-grown $REBa_2Cu_3O_{y-x}$ bulk superconductors *Supercond. Sci. Technol.* **13** 1202–13

[13] Koblischka M R and Murakami M 2000 Pinning mechanisms in bulk high-T_c superconductors *Supercond. Sci. Technol.* **13** 738–44

[14] Shlyk L, Krabbes G, Fuchs G, Nenkov K and Verges P 2003 Melt-textured $YBa_2Cu_3O_7$ based material doped with Li: high trapped fields and pinning *Phys. C: Supercond.* **392–396** 540–4

[15] Ishi Y, Yamazaki Y, Nakashima T, Ogino H, Shimoyama J, Horii S and Kishio K 2008 Chemical (Sr,Co)-doping effect on critical current density for Dy123 melt-solidified bulks *Mater. Sci. Eng.* B **151** 69–73

[16] Pavan Kumar Naik S, Muralidhar M, Jirsa M and Murakami M 2017 Growth and physical properties of top-seeded infiltration growth processed large grain (Gd,Dy)BCO bulk superconductors *J. Appl. Phys.* **122** 193902

[17] Volochova D, Antal V, Piovarci S, Kováč J, Jirsa M, Noudem J G and Diko P 2016 Microstructure and superconducting properties of YBCO bulk superconductors with RE substitutions *IEEE Trans. Appl. Supercond.* **26** 7200604

[18] Volochova D, Antal V, Kovac J and Diko P 2017 YBCO bulk superconductors with Sm addition *Mater. Sci. Forum* **891** 483–8

[19] Volochova D, Jurek K, Radusovska M, Piovarci S, Antal V, Kovac J, Jirsa M and Diko P 2014 Contamination of YBCO bulk superconductors by samarium and ytterbium *Phys. C. Supercond. Appl.* **496** 14–7

[20] Vojtkova L, Diko P and Rajňák M 2018 Influence of Sm_2O_3 and La_2O_3 additions on the microstructure and properties of YBCO bulk superconductors prepared by TSIG process *IEEE Trans. Appl. Supercond.* (https://doi.org/10.1109/TASC.2018.2797981)

[21] Bean C P 1962 Magnetization of hard superconductors *Phys. Rev. Lett.* **8** 250–3

[22] Uhlman D R, Chalmers B and Jackson K A 1964 Interaction between particles and a solid-liquid interface *J. Appl. Phys.* **35** 2986–93

[23] Endo A, Chauhan H S, Egi T and Shiohara Y 1996 Macrosegregation of $Y_2Ba_1Cu_1O_5$ particles in $Y_1Ba_2Cu_3O_{7-\delta}$ crystals grown by an undercooling method *J. Mater. Res.* **11** 795–803

[24] Lifshitz I M and Slyozov V V 1961 The kinetics of precipitation from supersaturated solid solutions *J. Phys. Chem. Solids* **19** 35–50